Pharm Res (2011) 28:2204–2222
DOI 10.1007/s11095-011-0448-z

RESEARCH PAPER

Turbidity Spectroscopy for Characterization of Submicroscopic Drug Carriers, Such as Nanoparticles and Lipid Vesicles: Size Determination

Mustafa M. A. Elsayed • Gregor Cevc

Received: 25 December 2010 / Accepted: 7 April 2011 / Published online: 17 May 2011

ABSTRACT

Purpose To apply UV/Vis spectrometry for characterization of submicroscopic drug carriers, such as nanoparticles and lipid vesicles.

Methods We first investigated theoretically, within the framework of the Rayleigh-Gans-Debye approximation (RGDA), parameters affecting turbidity spectrum, $\tau(\lambda)$, of nanosized light scatterers. We then analyzed, within the framework of the RGDA, experimental turbidity spectra ($\lambda =$ 400–600 nm) of extruded unilamellar vesicle (70 nm $\leq 2r \leq$ 110 nm) suspensions to derive vesicle size, using dynamic light scattering results for comparison. We similarly studied the preparations polydispersity and lamellarity and monitored vesicle size changes.

Results Turbidimetry suffices for accurate, fast, and viscosity-independent characterization of submicroscopic particles. Analysis of turbidity spectra, or more precisely wavelength exponent spectra (derivatives of logarithmic turbidity spectra), yielded similar average radii ($r = 54.2 \pm 0.2$ nm; 46.0 ± 0.2 nm; 35.5 ± 0.1 nm) as dynamic light scattering ($r = 55.9 \pm 1.5$ nm; 46.1 ± 0.4 nm; 36.1 ± 0.4 nm). Both methods also revealed similar suspension polydispersity and cholate-induced vesicle size changes in a few nanometer range.

Conclusion Despite its experimental simplicity, the widely accessible turbidimetric method provides accurate size values and is suitable for (continuous) monitoring size stability, or sameness, of submicroscopic drug carriers.

KEY WORDS continuous monitoring · drug delivery · light scattering · product quality control · size distribution

INTRODUCTION

Submicroscopic particles/aggregates, such as nanocrystals (1,2), nanoparticles (3,4), polymeric micelles (5), nanoemulsions (2,6,7), or lipid bilayer vesicles (liposomes), are gaining popularity in the pharmaceutical field. For example, lipid bilayer vesicles are now often used in drug delivery, gene therapy, and diagnostics (8,9), and as membrane models (10). Size and size distribution critically influence all applications of submicroscopic particles and are particularly important in the pharmaceutical field. A plethora of techniques has thus been used to study size of particulate drug carriers, but only a few such techniques found their way out of specialized laboratories.

The most obvious and conceptually simplest method for studying shape, size, and size distribution of submicroscopic particles is electron microscopy. The method is costly, laborious, and skill-demanding, however. It involves analysis of particles outside their actual dispersion medium and is often subject to sample perturbation and preparation artifacts. It moreover requires taking and inspecting many electron micrographs to gain a representative result. Electron microscopy is therefore mainly employed in research, especially for studying particles with an unusual

M. M. A. Elsayed
IDEA AG, Frankfurter Ring 193a, 80807 Munich, Germany

M. M. A. Elsayed
Department of Pharmaceutics, Faculty of Pharmacy
Alexandria University, El-Khartoum Square, El-Azarita
Alexandria 21521, Egypt
e-mail: mmaelsayed@gmail.com

G. Cevc (✉)
Advanced Treatments Institute, Tassilostr. 3
82131 Gauting, Germany
e-mail: cevc@advanced-treatments.org

or changing shape, or else a broad size distribution. Other kinds of high resolution microscopy, such as the scanning tunneling microscopy (11) or the atomic force microscopy (12,13), which can resolve structures at nanometer or sub-nanometer scale, are even more expensive and complex to deal with.

Some scattering techniques can also highlight carrier size and shape characteristics. The explorable length-scale depends primarily on the employed light/radiation wavelength. The small-angle scattering of X-rays and neutrons typically resolves structures measuring 1 nm to 100 nm in size (14–19). Such limited explorable size, the high cost of the involved equipment, and/or the scarcity of suitable radiation sources restricts applicability of such scattering techniques in the pharmaceutical field. Submicroscopic, nanosized[1] drug carriers are thus typically characterized with the longer optical/visible wavelengths.

The dynamic light scattering (DLS), which is also known as quasi-elastic light scattering or photon correlation spectroscopy (PCS), is currently the most popular method for measuring size of submicroscopic particles, including nanosized drug carriers (20–22). The technique requires no special skill to use. However, it does involve not inexpensive instruments that are therefore not broadly accessible. Furthermore, it typically takes at least 30 s and often longer to collect data for a single good-quality DLS measurement; dynamic light scattering therefore cannot monitor rapid size changes. Finding a less costly, more accessible, and potentially faster method for size characterization of colloidal drug carriers is thus desirable.

The static light scattering (SLS) can also provide information about size and, to an extent, shape of light scattering particles. Extraction of such information normally involves analyzing the angular dependency of light scattering. The Guinier-plot (approximation for small-angle data (23)) or the Zimm-plot (24,25) affords the scatterer radius of gyration (26–29). Fitting the angular dependency of the scattered light intensity, $I(\theta)$, with a suitable form-factor and size-distribution function reveals the underlying size-distribution. Such fitting can moreover provide information about the scattering particle structure, including spherical shell/lipid vesicle bilayer thickness (29). Combining the Zimm-plot and the Rayleigh-Gans-Debye approaches provides even more accurate values for these particle characteristics (30). A combination of light scattering with flow field-flow fractionation yields absolute size distribution (31). All these analytical procedures involve analysis of angular dependency of light scattering and thus depend on rather special and expensive pieces of equipment, including a goniometer or an array-detector.

Heller and colleagues quite early (32–35) proposed using differential turbidity spectra—in other words, wavelength dependency of light scattering—for size characterization of submicroscopic particles. The concept relies on dependency of the scattering vector, $q(\theta,\lambda) = (4\pi n/\lambda)\sin(\theta/2)$, on both the scattering angle, θ, and the incident light wavelength, λ (n being the dispersion medium refractive index).

Analysis of turbidity spectrum, $\tau(\lambda)$, which for a non-absorbing sample corresponds to extinction spectrum, is attractive for several reasons: *i*) it requires only a simple, broadly accessible UV-Vis spectrophotometer to collect experimental data; *ii*) it allows monitoring of size changes on time scale of the order of 5–10 s with a conventional spectrophotometer and much faster with an instrument equipped with a multi-channel detector; *iii*) the method is simple yet sensitive. All these advantages notwithstanding, turbidity spectrum analysis has attracted little attention to date, especially in the field of drug carrier research. Only a few practical characterization attempts were published to date (36–39) and, at least for lipid vesicles, were quantitatively unsuccessful; this is possibly due to some underlying theoretical and/or experimental problems. We considered these problems and in this publication show how turbidity spectrum analysis can be successfully applied in the pharmaceutical field for the purpose of particulate drug carrier characterization.

In the following text, we first scrutinize the theoretical background of turbidity spectrum analysis within the framework of the Rayleigh-Gans-Debye approximation. We study effects of colloidal suspension characteristics on $\tau(\lambda)$ and provide all equations necessary for extracting the most relevant characteristics from such spectra. We illustrate the advocated analytical method using suspensions of lipid bilayer vesicles, also addressing bilayer thickness and lamellarity effects on turbidity spectrum. We juxtapose the outcome of turbidity spectrum and corresponding dynamic light scattering analyses for various lipid vesicle suspensions to show how important colloid descriptors can be deduced from the measured turbidity or wavelength exponent spectra and to prove an excellent match between results of both analytical approaches.

THEORY

Description of a Light Scattering Particle Suspension

A homogeneous spherical particle is completely described as a light scatterer in terms of its refractive index, n_P, and radius, r. The latter defines the surface area, $A=4\pi r^2$, and

[1] The word "nanosized" herein implies diameters between 10 and a few hundred nanometers.

volume, $V=(4\pi/3)r^3$, of a single scattering particle. The number concentration of such homogeneous particles in suspension, i.e. the number of spherical particles per unit volume of the suspension, is then

$$\mathcal{N}_P = \frac{C}{V\rho}, \tag{1}$$

C being the particle material concentration (*weight/volume*) and ρ the particle density.

Describing a hollow sphere/spherical shell as a light scatterer requires knowledge of the core and the shell refractive indices, n_{core} and n_{shell}; the shell outer radius, r_{shell}; and the shell thickness, d_{shell}. If one uses the corresponding single shell volume, $V = (4\pi/3)(r_{shell}^3 - r_{core}^3)$, with $r_{core} = r_{shell} - d_{shell}$, in Eq. 1, one can also calculate the number concentration of hollow spheres/spherical shells in a suspension from the expression.

Vesicles are exemplary hollow spherical particles (28,29,36). Mathematical description of bilayer vesicles as spherical shells (Fig. 1) relies on the vesicle/particle outer radius, r_v; the number of bilayers/shells per vesicle/particle, $l \geq 1$; the bilayer/shell thickness, d_b; the inter-bilayer/-shell water layer thickness, d_w; and the lipid/shell refractive index, n_L. If we identify the innermost bilayer/shell with $x=1$ and the outermost bilayer/shell with $x = l$, the outer radius of the x-th bilayer/shell is given by

$$r_{x,out} = r_v - [(l-x)(d_b + d_w)]. \tag{2}$$

The inner radius of the same bilayer/shell is accordingly

$$r_{x,in} = r_{x,out} - d_b. \tag{3}$$

The total (outer + inner) surface area of all bilayers/shells in a vesicle/particle is thus

$$A_{L,v} = 4\pi \sum_{x=1}^{x=l} \left[r_{x,out}^2 + r_{x,in}^2 \right]. \tag{4}$$

For a single-bilayer (unilamellar) vesicle or a single-shell particle Eq. 4 simplifies to

$$A_{L,v} = 4\pi \left[r_v^2 + (r_v - d_b)^2 \right]. \tag{5}$$

The number concentration of bilayer vesicles/spherical shell particles in a suspension then becomes in mathematical terms

$$\mathcal{N}_v = \frac{\mathcal{N}_A A_L L}{A_{L,v}}, \tag{6}$$

where $\mathcal{N}_A$ is the Avogadro's number (6.02205×10^{23} mol^{-1}), A_L the average area of (lipid) molecules forming bilayers/shells, and L the molar concentration of such, essentially water-insoluble, molecules. The subscript v clarifies that Eq. 6, applicable to vesicles, differs from Eq. 1, useful for calculating the number concentration of solid particles in a suspension. Phosphatidylcholine molecules in a fluid/liquid crystalline phase typically occupy an area 0.55 nm$^2 \leq A_L \leq$ 0.70 nm^2 (40–42). In the gel phase the area is appreciably smaller and is normally in the range 0.42 nm$^2 \leq A_L \leq$ 0.55 nm^2. One can follow Luzzati by identifying the molecular area upper limit with $A_L = 2V_L/d_b$, i.e. by postulating constancy of the easily measurable volume of a single lipid molecule, V_L. Some area and volume data for different phospholipids, phases, and temperatures were published (43).

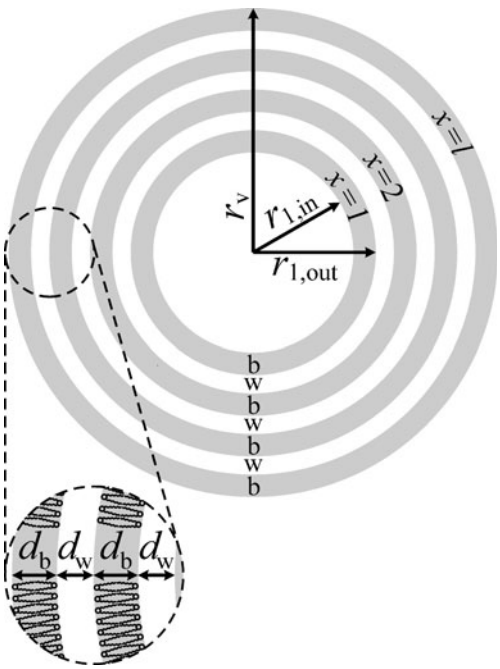

Fig. 1 Schematic representation of a multibilayer vesicle. r_v is the vesicle outer radius, d_b the bilayer/shell thickness, d_w the inter-bilayer/-shell water layer thickness, and $l \geq 1$ the number of bilayers/shells per vesicle. The innermost bilayer is identified with $x = 1$ and the outermost bilayer with $x = l$.

Theory of Light Scattering

We herein analyze turbidity spectra within the framework of the Rayleigh-Gans-Debye approximation (RGDA). One fundamental assumption of the approximation is absence of a significant light "phase shift," expressed mathematically as $2ka(m-1) \ll 1$. $k = 2\pi n/\lambda$ is the propagation constant in the dispersion medium, n the

dispersion medium refractive index, and λ the incident light wavelength in vacuum. a is a characteristic dimension of the light scattering particle; for a sphere it denotes the radius r. $m = n_P/n$ is the particle-to-dispersion medium relative refractive index, with n_P denoting the scattering particle refractive index. In practice, this means that the RGDA is only valid for scattering particles much smaller than $\lambda/[n(m-1)]$. The size range amenable to the RGDA correspondingly widens when the dispersion medium refractive index approaches the scattering particle refractive index, i.e. $m-1 \to 0$ (see Appendix A). When the RGDA basic condition is not met, one must revert to the more general and exact, but also more complex, Mie-theory of light scattering (44–46).

Within the framework of the Rayleigh-Gans-Debye approximation, the scattered light intensity can be written as (36,45–47)

$$I(\theta,\lambda) = I_0 N \left(\frac{3\pi V}{d}\right)^2 \left(\frac{n(\lambda)}{\lambda}\right)^4 \left(\frac{m^2(\lambda)-1}{m^2(\lambda)+2}\right)^2 \left(\frac{1+\cos^2\theta}{2}\right) P(\theta,\lambda). \tag{7}$$

I_0 is the incident light intensity and N the number concentration of the light scattering particles (i.e. N_P or N_v). V is the volume of an individual particle, d the observation distance (i.e. the distance between the scattering particle and the detector), and θ the scattering angle. The scattering or form factor, $P(\theta,\lambda)$, in Eq. 7 allows for the scattering particle finite size and non-sphericity; it accounts for interference of light scattered from different parts of the scattering particle. This factor consequently depends on the scattering particle shape. We provide the form factors for the most frequently studied particle geometries (homogeneous sphere, concentric/coated sphere, and hollow sphere/spherical shell) in the following subsections. The form factors pertaining to other particle geometries (e.g. cylinder, rod, disk, cube, ellipsoid, or prolate vesicle) were published as well (27,30,45,48). Scattering particles appreciably smaller than the incident light wavelength have $P(\theta,\lambda) \to 1$ (i.e. Rayleigh scattering). Wavelength and angular dependency of the light scattered by such particles therefore contain no structural information.

Integrating over the surface of a sphere yields the total light scattered or turbidity (36):

$$\begin{aligned}\tau(\lambda) &= 2.303\mathrm{OD} \\ &= 9N\pi^3 V^2 \left(\frac{n(\lambda)}{\lambda}\right)^4 \left(\frac{m^2(\lambda)-1}{m^2(\lambda)+2}\right)^2 \int_0^\pi (1+\cos^2\theta) P(\theta,\lambda) \sin\theta \mathrm{d}\theta.\end{aligned} \tag{8}$$

OD is the optical density, as measured with a spectrophotometer for a non-absorbing sample in a cuvette with 1 cm path-length.[2]

We define the derivative of the logarithmic turbidity spectrum as

$$w(\lambda) = -\frac{\mathrm{d}}{\mathrm{d}\log\lambda} \log\tau(\lambda). \tag{9}$$

Differentiation of Eq. 8 gives

$$w(\lambda) = 4 - \frac{\mathrm{d}}{\mathrm{d}\log\lambda} \log\left[n^4(\lambda)\left(\frac{m^2(\lambda)-1}{m^2(\lambda)+2}\right)^2 \int_0^\pi (1+\cos^2\theta) P(\theta,\lambda)\sin\theta \mathrm{d}\theta\right]. \tag{10}$$

Equation 10 considers the wavelength dependency of refractive indices (see Appendices C and D), the pertinent form factor, and consequently the logarithmic turbidity spectrum derivative w.

Turbidity is commonly written as a power function of the incident light wavelength: $\tau(\lambda) \sim \lambda^{-w}$ (32,33). This approximate expression neglects the wavelength dependency of w and thus does not exactly match our definition of w (Eqs. 9–10), despite the similar general meaning. This difference notwithstanding, we use in this text the succinct term "wavelength exponent spectrum" to describe $w(\lambda)$ as defined in Eqs. 9–10.

Homogeneous Sphere

For an optically homogeneous sphere the form factor is (45,49,50)

$$P(\theta,\lambda) = \left[\frac{3(\sin\ qr - qr\ \cos\ qr)}{q^3 r^3}\right]^2, \tag{11}$$

where the scattering vector is again $q(\theta,\lambda) = (4\pi n/\lambda)\ \sin(\theta/2)$. Such form factor applies to a sphere or a reasonably homogeneous spherical hetero-aggregate, such as particles in a nanoemulsion.

[2] Optical density is the quantity commonly provided by a spectrophotometer according to the definition $\mathrm{OD} = -\log(I_T/I_0)/b$, where I_T is the transmitted light intensity, I_0 the incident light intensity, and b the optical path-length. OD corresponds to extinction or total attenuation, i.e., due to absorption + scattering. The term "absorbance," A, denotes attenuation due to absorption, i.e. for an absorbing, non-scattering sample $\mathrm{OD} = A$. The term "turbidity," τ, denotes attenuation due to scattering. The most common definition of turbidity, which we use herein, is based on the natural rather than the decadic logarithm, $\tau = -\ln(I_T/I_0)/b$, however. Accordingly, for a non-absorbing sample, $\tau = 2.303$ OD. Before applying Eq. 8, one should thus check whether the used spectrophotometer provides τ or OD, as defined here.

Sphere Coated with a Spherical Shell

For a spherical particle comprising two concentric and optically homogeneous regions, i.e. a spherical core of one medium encased in a concentric spherical shell of a different medium, the form factor is (45,51)

$$P(\theta,\lambda) = \left[\frac{3\left[\left(\sin\ qr_{\text{shell}} - qr_{\text{shell}}\cos\ qr_{\text{shell}}\right) + \frac{m_{\text{core}}(\lambda)-m_{\text{shell}}(\lambda)}{m_{\text{shell}}(\lambda)-1}\left(\sin\ qr_{\text{core}} - qr_{\text{core}}\cos\ qr_{\text{core}}\right)\right]}{q^3 r_{\text{shell}}^3}\right]^2. \quad (12)$$

r_{core} denotes the core radius, r_{shell} the shell outer radius, m_{core} the core-to-dispersion medium relative refractive index, and m_{shell} the shell-to-dispersion medium relative refractive index. When Eq. 12 is used, the total volume, $V = (4\pi/3)r_{\text{shell}}^3$, and the shell-to-dispersion medium relative refractive index, i.e. $m(\lambda) = m_{\text{shell}}(\lambda)$, must be used in Eqs. 7, 8, and 10.

Hollow Sphere/Spherical Shell

The form factor pertaining to a shell-coated sphere simplifies to the expression for a hollow sphere/spherical shell when $m_{\text{core}} = 1$:

$$P(\theta,\lambda) = \left[\frac{3(\sin\ qr_{\text{shell}} - qr_{\text{shell}}\cos\ qr_{\text{shell}} - \sin\ qr_{\text{core}} + qr_{\text{core}}\cos\ qr_{\text{core}})}{q^3 r_{\text{shell}}^3}\right]^2. \quad (13)$$

Again, the total sphere volume: $V = (4\pi/3)r_{\text{shell}}^3$ and the shell-to-dispersion medium relative refractive index, i.e. $m(\lambda) = m_{\text{shell}}(\lambda)$, must be used in Eqs. 7, 8, or 10.[3]

The form factor described by Eq. 13 applies to spherical unilamellar lipid bilayer vesicles. For such vesicles the parameter r_{shell} in Eq. 13 corresponds to the vesicle radius, $r_{\text{shell}} = r_{\text{v}}$. The aqueous core radius is $r_{\text{core}} = r_{\text{v}} - d_{\text{b}}$, d_{b} being bilayer thickness. $m(\lambda) = m_{\text{shell}}(\lambda)$ is the bilayer-to-dispersion medium relative refractive index.

For a multilamellar vesicle the form factor becomes (36)

$$P(\theta,\lambda) = \left[\frac{3\sum_{x=1}^{x=l}\left[\sin\ qr_{x,\text{out}} - qr_{x,\text{out}}\cos\ qr_{x,\text{out}} - \sin\ qr_{x,\text{in}} + qr_{x,\text{in}}\cos\ qr_{x,\text{in}}\right]}{q^3 r_{\text{v}}^3}\right]^2, \quad (14)$$

$r_{x,\text{out}}$, $r_{x,\text{in}}$, x, and l being defined in the "Description of a Light Scattering Particle Suspension" section. In combination with Eq. 14, the total vesicle volume and the shell-to-dispersion medium relative refractive index must be used in Eqs. 7, 8, or 10.

Size Distribution

To describe light scattering by a real population of particles, one must consider particle size distribution as well. Several distribution functions were proposed to meet the goal. Herein, we are using the log-normal distribution function:

$$f^{\text{Num}}(r) = \frac{1}{r\delta\sqrt{2\pi}}\exp\left[\frac{-[\ln r - \mu]^2}{2\delta^2}\right], \quad (15)$$

which postulates that the size logarithm, ln r, rather than the size itself, r, is normally distributed. μ is the mean value of ln r and δ the corresponding standard deviation of ln r. Correspondingly, $\mu = \ln \bar{r}_{\text{g}}$ and $\delta = \ln \sigma_{\text{g}}$, where $\bar{r}_{\text{g}}$ is the geometric mean and σ_{g} the geometric standard deviation of r. Equation 15 satisfactorily describes size distribution in a suspension of natural particles (45) and is also acceptable for lipid vesicles.

Popular alternatives to the log-normal distribution function are the Weibull (31,53,54) and the gamma (28) distribution functions. While the log-normal (Eq. 15) and the gamma distribution functions are two-parametric and thus simpler to use, the Weibull distribution function is three-parametric and can thus provide more robust and correct estimates for the lower size limit. Compared to the log-normal distribution, the Weibull distribution hence better describes especially small (e.g. sonicated (53,54) or extruded (31)) liposome size distribution.

Allowance for scatterer size distribution transforms Eqs. 7 and 8 into

$$I(\theta,\lambda) = \frac{I_0 N}{2}\left(\frac{3\pi}{d}\right)^2\left(\frac{n(\lambda)}{\lambda}\right)^4\left(\frac{m^2(\lambda)-1}{m^2(\lambda)+2}\right)^2\int f^{\text{Num}}V^2\left(1+\cos^2\theta\right)P(\theta,\lambda)\,\text{d}r, \quad (16)$$

$$\tau(\lambda) = 9N\pi^3\left(\frac{n(\lambda)}{\lambda}\right)^4\left(\frac{m^2(\lambda)-1}{m^2(\lambda)+2}\right)^2\int f^{\text{Num}}V^2\int_0^{\pi}\left(1+\cos^2\theta\right)P(\theta,\lambda)\sin\,\theta\,\text{d}\,\theta\,\text{d}r. \quad (17)$$

[3] It is noteworthy that such a form factor is commonly (27–30,38,48,52) written with $q^3\left(r_{\text{shell}}^3 - r_{\text{core}}^3\right)$ instead of $q^3 r_{\text{shell}}^3$ in the denominator. In contrast to our treatment for the particles as hollow spheres, the same particles are in such approach treated as spherical shells; shell volume: $V = (4\pi/3)\left(r_{\text{shell}}^3 - r_{\text{core}}^3\right)$ must then be used in Eq. 7 or 8.

One should be mindful of the r-dependency of f^{Num}, V, and P too. The corresponding number concentration for homogeneous spheres and spherical shells (cf. Eq. 1) is

$$\mathcal{N}_{\mathrm{P}} = \frac{C}{\rho \int f^{\mathrm{Num}} V \, \mathrm{d}r}. \tag{18}$$

For spherical vesicles (cf. Eq. 6) this more specifically means

$$\mathcal{N}_{\mathrm{v}} = \frac{\mathcal{N}_{\mathrm{A}} A_{\mathrm{L}} L}{\int f^{\mathrm{Num}} A_{\mathrm{L,v}} \mathrm{d}r}. \tag{19}$$

Hitherto, we have considered only the number-weighed size distribution. Researchers commonly express size distributions derived from light scattering experiments as intensity-weighed size distributions, however. To get the latter kind of distribution, one should divide the contribution of each scatterer with radius r to the sample turbidity by the overall suspension turbidity. If one then fits the intensity-weighed size distribution to the log-normal distribution function, one gets the intensity-weighed mean scatterer size.

MATERIALS AND METHODS

Materials

We purchased soybean phosphatidylcholine (SPC, Lipoid S 100, purity = 97.8%, the assumed average molecular weight ~800 g/mol) from Lipoid GmbH (Ludwigshafen, Germany). Sodium cholate hydrate (purity ≥97%) was from Sigma-Aldrich (Steinheim, Germany). All other chemicals and reagents were of analytical grade. Polycarbonate membranes were from GE Water & Process Technologies (Trevose, PA, U.S.A.).

Preparation of Lipid Vesicles

We prepared unilamellar vesicles of different size by extrusion. In brief, we dissolved the necessary phospholipid amount in chloroform, in a 500 mL round-bottom flask and removed the solvent at 50°C in a rotary evaporator to get a thin lipid film, which we hydrated at the same temperature with distilled water. This prompted spontaneous formation of multilamellar vesicles. The resulting suspension had total phospholipid concentration of 120 mg/g (~150 mmol/kg).

To produce the more uniform unilamellar vesicles, "V80," we extruded the original multilamellar vesicle suspension 20 times through a set of polycarbonate membranes with 80 nm pores under 1.5 MPa nitrogen gas pressure. To gain the smaller unilamellar vesicles, "V50," we further extruded the "V80" suspension 16–20 times through a set of polycarbonate membranes with 50 nm pores under nitrogen gas pressure of 2.1 MPa. To obtain the smallest studied unilamellar vesicles, "V30," we finally extruded the "V50" suspension 16–20 times through a set of polycarbonate membranes with 30 nm pores under nitrogen gas pressure of 2.5 MPa. To prepare suspensions with different lipid concentrations, we diluted the starting suspensions with distilled water which we pre-filtered through a syringe filter with 200 nm pore diameter to eliminate large dust particles.

We verified that the described extensive extrusion did not eliminate a considerable amount of lipid material, i.e. did not appreciably reduce the final lipid concentration. For this purpose, we measured phosphatidylcholine concentration in representative preparations with HPLC. We used an in-house modification of the method described by Nasner and Kraus (55) with refractive index detection (56).

Monitoring Effect of Cholate on Lipid Vesicles

We applied the turbidimetric method to monitor lipid vesicle size changes induced by addition of sodium cholate as a function of the surfactant concentration. We first prepared a series of vesicle suspensions with 8 mmol lipid/kg in an aqueous carbonate buffer (50 mM, pH = 10.25) adjusted with NaCl to a final ionic strength of 150 mM. We always prepared fresh samples immediately before starting an experimental series to minimize lipid degradation/hydrolysis at the high chosen pH. We moreover used the HPLC assay described earlier to confirm that no detectable phosphatidylcholine hydrolysis took place during experiments: the lysophosphatidylcholine level in several representative samples kept at pH = 10.25 and T = 25°C for 6 h was below the HPLC method detection limit. Total phosphatidylcholine concentration also did not change. We prepared a series of sodium cholate solutions/suspensions with different concentrations in a similar buffer and adjusted each preparation to a final ionic strength of 150 mM with NaCl.

We then mixed an aliquot of the test vesicle suspension with an equal volume of the appropriate sodium cholate solution/suspension and stirred the blend thoroughly. All mixtures had final lipid concentration of 4 mmol/kg and final cholate concentration between 0.0 and 1.2 mmol/kg. We equilibrated all mixtures at room temperature (~25°C) for 3 h, which sufficed for reaching quasi-equilibrium (a constant optical density or turbidity reading) in the studied cholate concentration range (57). Finally, we recorded the suspensions turbidity spectra (λ = 400–600 nm).

Turbidity/Optical Density Measurements

We measured optical density (extinction) spectra mainly with a Shimadzu UV-1601 double-beam UV-Vis spectro-

photometer equipped with a six-position, automated sample changer and the Shimadzu UVProbe version 2.0 software (Shimadzu Corporation, Kyoto, Japan); we will refer to this instrument as "Spectrophotometer A." To test the general validity and ruggedness of the method, we also recorded optical density spectra of selected samples with a PerkinElmer Lambda EZ 201 UV-VIS spectrophotometer equipped with the PESSW version 1.2 (Revision E) software; we will refer to this instrument as "Spectrophotometer B." We first confirmed negligible light absorbance by SPC in the employed concentration range at wavelengths above 400 nm. We then recorded optical density spectra at $\lambda = 400$–600 nm. Both spectrophotometers (A and B) produced comparably useful spectra, measured with the test samples in a conventional, 1-cm light-path quartz cuvette. We moreover measured some optical density spectra with another spectrophotometer that works with much smaller volumes (5 μL). This spectrophotometer (NanoDrop®1000, Thermo Scientific), which has an air-exposed measuring site, produced too noisy spectra for reliable size determination, however.

We programmed a Mathcad sheet (Mathcad version 14, Parametric Technology Corporation, Needham, Massachusetts, USA) including the complete set of equations given in Theory section. We used the Levenberg-Marquardt non-linear regression algorithm to derive vesicle size. Before analyzing the measured turbidity spectra with the method, we confirmed that the spectra are in the linear concentration dependency range (i.e. $d\tau/dL$ = constant), which is a prerequisite for applying Eq. 8 or Eq. 17 (see the Theory section). We also confirmed that the investigated vesicles sizes were below the r-limit above which $w(\lambda)$ oscillates as a function of r. This avoids ambiguous non-linear regression results (see Results and Discussion, Experimental Recommendations and Limitations, and Appendix B).

Dynamic Light Scattering (Photon Correlation Spectroscopy)

For the dynamic light scattering measurements we employed an ALV-NIBS/HPPS particle sizer (ALV-Laser Vertriebsgesellschaft mbH, Langen, Germany), equipped with a HeNe laser ($\lambda = 632.8$ nm) and operating at a scattering angle of 173°. We measured each sample at 25°C three to six times and then analyzed the results with the ALV-5000/E/EPP software (version 3.0, regularized fit routine, scattering spherical shells) based on the CONTIN 2DP method (58,59). We took the refractive index and the dynamic viscosity of water at 25°C to be $n = 1.33162$ ($\lambda = 632.8$ nm; Eqs. C1–C2) and $\eta = 0.89038$ cP. We calculated the dynamic viscosity of the aqueous carbonate buffer (for the samples used to monitor the effect of cholate on vesicle size) with the formula developed by Pereira *et al.* (60) to be 0.91711 cP. The effect of sodium cholate on suspension viscosity in the studied concentration range was negligible (<0.002 cP) (61).

RESULTS AND DISCUSSION

Characteristics Affecting Turbidity of a Nanosized Particle Suspension

In this section, we explore theoretically effects of various particle and dispersion medium characteristics on turbidity and wavelength exponent spectra of a particle suspension, all within the framework of the Rayleigh-Gans-Debye approximation. We first focus on the general characteristics of any particle suspension; this includes particle mean size and size distribution, particle and dispersion medium refractive indices, and particle concentration within the homogeneous sphere as well as the hollow sphere models. We then deal with the special characteristics of hollow spheres/spherical shells/lipid vesicles, such as shell/bilayer thickness and number of shells/bilayers in a particle (i.e. lamellarity).

General Characteristics of a Nanosized Particle Suspension

Size. For a suspension of monodisperse (i.e. having the same size) particles with a fixed number concentration, the suspension turbidity increases with the particle size (Fig. 2, upper two panels). The effect is qualitatively similar for homogeneous and hollow spheres/vesicles. One can thus derive the average particle size from turbidity spectrum (Eq. 8) as long as the Rayleigh-Gans-Debye approximation assumptions are obeyed. Shorter wavelengths offer higher sensitivity.

The wavelength exponent, w, initially decreases with raising particle size (monodisperse particles, fixed number concentration; Fig. 2, lower two panels). When a certain size is reached, however, the wavelength exponent becomes an oscillating function of size (Appendix B, Fig. 11). The effect is qualitatively similar for homogeneous and hollow spheres/vesicles, but in quantitative detail depends on the scatterer geometry. One can consequently gain size information about the particles with a size below such limit (i.e. below the $w(\lambda,r)$ oscillations range) by analyzing wavelength exponent spectra using Eqs. 9–10. This includes all the vesicles studied experimentally in this work. Shorter wavelengths again offer higher sensitivity, whereas longer wavelengths permit studying larger particles (see Experimental Recommendations and Limitations and Appendix B).

Size Distribution. No real suspension is truly monodisperse. To allow for particle size distribution, we introduced the log-normal distribution function into the mathematical

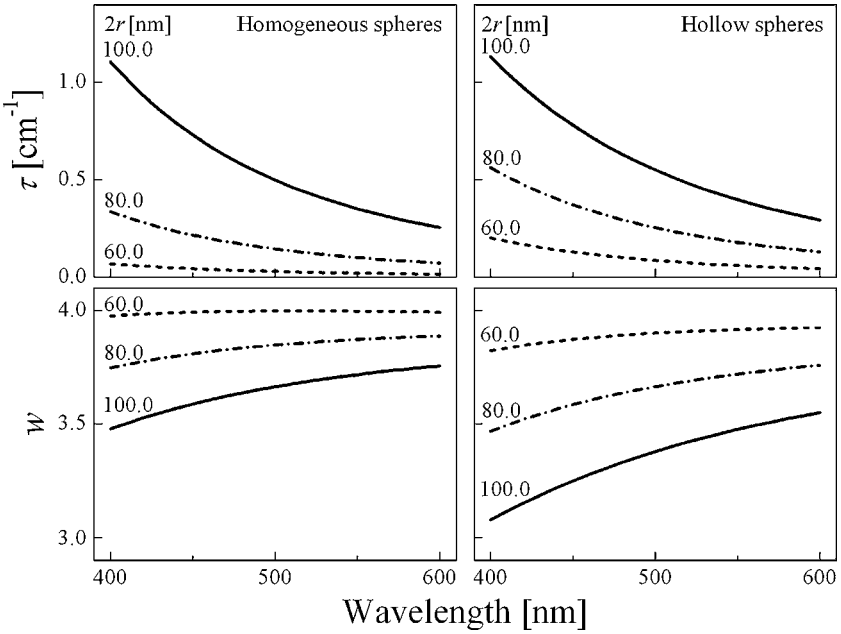

Fig. 2 Effect of light scattering particle diameter ($2r = 60.0$–100.0 nm, monodisperse) on the particle suspension turbidity (*upper panels*) and wavelength exponent (*lower panels*) spectra. The curves were calculated for suspensions of either homogeneous spheres (*left two panels*, number concentration $N_P = 1.1 \times 10^{12}$ mL^{-1}) or hollow spheres/spherical shells/lipid vesicles (*right two panels*, number concentration $N_v = 3.5 \times 10^{13}$ mL^{-1}, shell thickness $d_{shell} = 3.6$ nm). The homogeneous spheres and the spherical shells/lipid bilayers were assumed to have the refractive index of dipalmitoylphosphatidylcholine (Eq. D1) and the dispersion medium to have the refractive index of water (Eqs. C1–C2).

expressions used for various analyses (see the Theory section). Our results thus give the geometric, rather than arithmetic, mean diameters and standard deviations. Simulations described in this section and the consequent findings are accordingly quantitatively valid only within limits of such distribution function applicability.

Broadening the size distribution (i.e. increasing the standard deviation, σ_g) in a suspension of particles with fixed mean diameter and number concentration increases the suspension turbidity and decreases the wavelength exponent. Fig. 3 illustrates the effects for suspensions of homogeneous spheres, but we also got similar results for hollow spheres (data not shown). Broadening size distribution (Fig. 3) and increasing mean particle diameter (Fig. 2) influence turbidity spectra similarly, at least in qualitative terms, for two main reasons: *i*) light scattering by a particle is a power function of the light scattering particle radius; higher turbidity caused by extending such particle size distribution towards the distribution function high end thus overcompensates the turbidity decrease caused by extending the size distribution towards the distribution function low end; *ii*) the log-normal distribution is skewed.

Quantitative analysis of a turbidity or wavelength exponent spectrum can afford the mean size as well as the size distribution width (expressed as a standard deviation) of suspended particles despite the qualitative similarity of effects of these two parameters. For illustration, we simulated a set of turbidity spectra ($\lambda = 400$–600 nm, Fig. 4, upper panel) for suspensions containing particles with different geometric mean diameter and standard deviation but identical turbidity at $\lambda = 600$ nm. We also generated a similar set of wavelength exponent spectra with identical wavelength exponent at $\lambda = 600$ nm (Fig. 4, lower panel). The spectra confirm that changing the mean diameter and standard deviation produces quantitatively dissimilar effects and yields characteristic $d\tau/d\lambda$ and $dw/d\lambda$ derivatives. These differences permit accurate calculation of the mean diameter and the corresponding standard deviation from the spectra. The analyzed spectrum broadening improves analytical accuracy.

Turbidity spectrum analysis neglecting scatterer size distribution (i.e. assuming monodispersity, $\sigma_g = 0$) provides a diameter value that is larger than the number-weighed geometric mean diameter and smaller than the intensity-weighed geometric mean diameter. Wavelength exponent spectrum analysis neglecting scatterer size distribution yields a good approximation of the intensity-weighted geometric mean diameter, provided that the underlying size distribution is not too wide (Table I).

Refractive Index. Suspension turbidity depends on the scattering particle and the dispersion medium refractive indices (Fig. 5). Raising the particle-to-dispersion medium relative refractive index, m, generally increases suspension turbidity. Wavelength exponent does not depend on the refractive indices values at any particular wavelength but

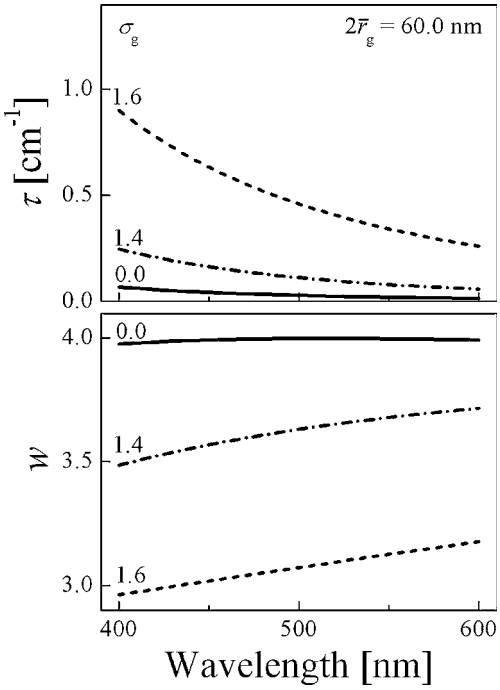

Fig. 3 Effect of particle size distribution width (geometric mean diameter $2\bar{r}_g = 60.0$ nm, standard deviation $\sigma_g = 0.0$–1.6 nm (equivalent to $\delta = 0.00$–0.45)) on suspension turbidity (*upper panel*) and wavelength exponent (*lower panel*) spectra. The curves were calculated for suspensions of homogeneous spheres with a number concentration $N_P = 1.1 \times 10^{12}$ mL^{-1}. The spheres were assumed to have the same refractive index as dipalmitoylphosphatidylcholine (Eq. D1) and the dispersion medium to have the refractive index of water (Eqs. C1–C2).

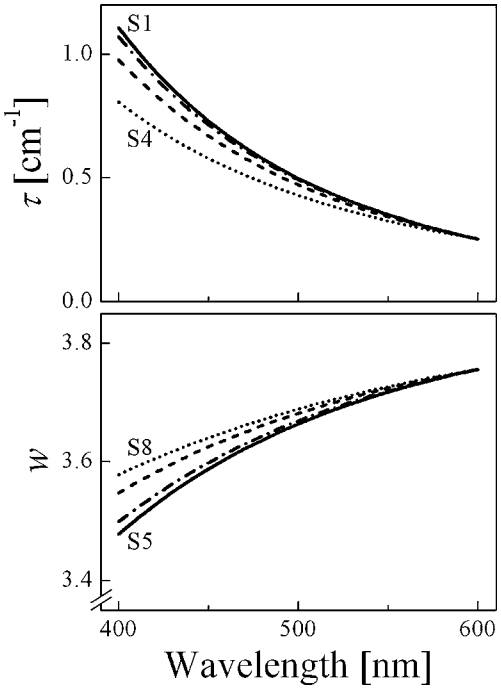

Fig. 4 Turbidity (*upper panel*) and wavelength exponent (*lower panel*) spectra calculated for suspensions of homogeneous spheres with constant number concentration $N_P = 1.1 \times 10^{12}$ mL^{-1} and variable geometric mean diameter and standard deviation. Detailed characteristics of the suspensions are given in Table I. The suspensions have either identical turbidity (*upper panel*) or wavelength exponent (*lower panel*) at $\lambda = 600$ nm. The figure illustrates how quantitative analysis of turbidity or wavelength exponent spectra can resolve the mean diameter as well as the standard deviation.

rather on their wavelength dependency (Eq. 15). The effect is usually positive. Tiny particles therefore have $\lim_{r \to 0} w > 4$. For an aqueous suspension of homogeneous spheres, assumed to have the same refractive index as dipalmitoylphosphatidylcholine (Eq. D1), in water (the refractive index calculated from Eqs. C1–C2), one gets $\lim_{r \to 0} w = 4.29$ at $\lambda = 400$ nm and $\lim_{r \to 0} w = 4.20$ at $\lambda = 500$ nm.

Concentration. Turbidity increases linearly with number concentration of particles in a suspension (Eq. 8). Linear concentration dependency of turbidity is thus a prerequisite for applying Eq. 8 for turbidity spectrum analysis. Indeed, any non-linearity is diagnostic of interference, for example, from quenching or multiple-scattering. Wavelength exponent is, in contrast, concentration independent (Eqs. 9–10). Inaccurate information about particle concentration, density, and/or molecular weight (for lipid vesicles, see Eqs. 1–6) consequently affects the outcome of turbidity spectrum analysis but not of wavelength exponent spectrum analysis. In turn, one can determine particle concentration by, first, calculating the average vesicle size from the wavelength exponent spectrum and, second, using this result to derive particle concentration from the corresponding turbidity spectrum, which is, unlike the former spectrum, sensitive to particle concentration.

Special Characteristics of Hollow Spheres/Spherical Shells/Lipid Vesicles

Shell/Bilayer Thickness. Hollow spheres scatter light more when their shell thickens. Turbidity of a suspension of monodisperse unilamellar vesicles with a fixed outer radius thus increases with bilayer thickness (Fig. 6, upper panel). The corresponding wavelength exponent is less affected by bilayer thickness. Within the 3–4 nm thickness range, which pertains to most common biological and synthetic lipids (Fig. 6, lower panel), the effect is close to nil. Inaccurate presumption about shell/bilayer thickness within such range thus produces significant errors (up to 100%) only if one derives hollow sphere/vesicle size from turbidity spectra. In contrast, similarly inaccurate presumption gives an error of less than 0.5 nm for hollow sphere/vesicle size calculated from corresponding wavelength exponent

Table I Characteristics of the Simulated Suspensions Used to Generate the Spectra Shown in Fig. 4

Line	Number-weighed[a]		Intensity-weighed[a,b]		Calculated (MD)[c]
	Mean diameter, $2\bar{r}_g$ [nm]	St. deviation, σ_g^d [nm]	Mean diameter, $2\bar{r}_g$ [nm]	St. deviation, σ_g^d [nm]	Diameter [nm]
Identical $\tau(\lambda = 600$ nm)[e]					
S1	100.0	0.0 (0.00)	100.0	0.0 (0.00)	100.0
S2	94.1	1.2 (0.02)	106.2	1.2 (0.02)	99.6
S3	78.7	1.3 (0.09)	125.4	1.3 (0.08)	98.4
S4	41.7	1.8 (0.36)	210.8	1.6 (0.24)	95.9
Identical $w(\lambda = 600$ nm)[f]					
S5	100.0	0.0 (0.00)	100.0	0.0 (0.00)	100.0
S6	86.5	1.2 (0.02)	97.8	1.2 (0.02)	99.2
S7	56.7	1.3 (0.09)	93.0	1.3 (0.08)	97.3
S8	14.9	1.8 (0.36)	97.8	1.6 (0.22)	96.2

[a] All calculations rely on the log normal distribution function; the table thus gives geometric, rather than arithmetic, mean diameters and standard deviations

[b] Calculated relying on turbidity at $\lambda = 500$ nm

[c] Diameters calculated by analyzing the simulated turbidity (Fig. 4, upper panel) or wavelength exponent (Fig. 4, lower panel) spectra presuming monodispersity, i.e. not allowing for particle size distribution

[d] Values in parenthese denote the conventional polydispersity index, defined as $PI = \delta^2 = (\ln \sigma_g)^2$

[e] Various suspensions of homogeneous spherical particles with the same turbidity at $\lambda = 600$ nm; the spheres were assumed to have the same refractive index as dipalmitoylphosphatidylcholine (Eq. D1) and the dispersion medium to have the refractive index of water (Eqs. C1–C2); number concentration $N_P = 1.1 \times 10^{12}$ mL^{-1}

[f] Various suspensions of homogeneous spherical partides with the same wavelength exponent at $\lambda = 600$ nm; the spheres were assumed to have the same refractive index as dipalmitoylphosphatidylcholine (Eq. D1) and the dispersion medium to have the refractive index of water (Eqs. C1–C2); number concentration $N_P = 1.1 \times 10^{12}$ mL^{-1}

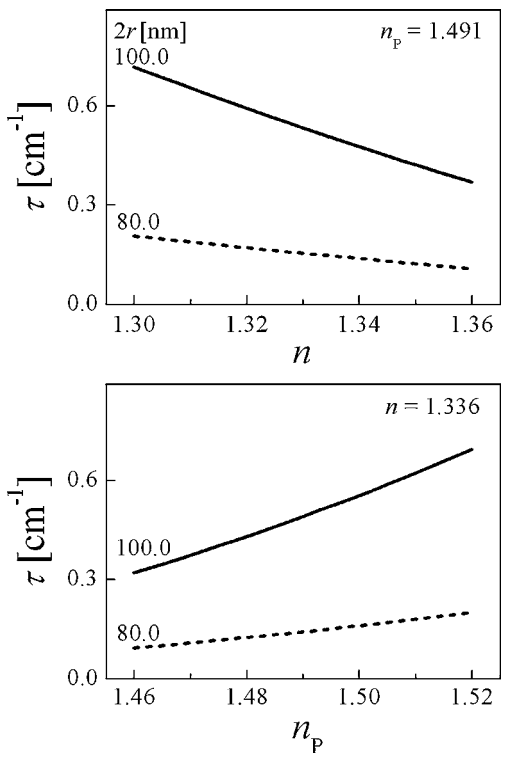

Fig. 5 Influence of particle and dispersion medium refractive indices on suspension turbidity. The curves were calculated at $\lambda = 500$ nm for suspensions of monodisperse ($2r = 80$ nm or 100 nm) homogeneous spheres with a number concentration $N_P = 1.1 \times 10^{12}$ mL^{-1}. Results for hollow spheres/spherical shells/lipid vesicles are qualitatively similar.

spectra.[4] Lacking trustworthy information about shell/bilayer thickness, one should therefore rely rather on wavelength exponent than on turbidity spectrum analysis for hollow sphere/vesicle size characterization.

Number of Shells/Lipid Bilayers (Lamellarity). Effect of increasing number of shells/bilayers on turbidity resembles that of increasing single shell/bilayer thickness. Vesicles with a higher number of bilayers (i.e. lamellarity, l) consequently produce more turbid suspensions at fixed lipid vesicle mass concentration[5], outer radius, and bilayer thickness (Fig. 7, upper panel). Wavelength exponent spectra change with lamellarity as well, but less so than turbidity spectrum (Fig. 7, lower panel).

Distribution of (Mixed) Lamellarity. A suspension of ideally uniform lipid vesicles comprises merely vesicles with identical lamellarity. Such a suspension is practically unachievable, however. We therefore assessed the influence of uncertain, or diverse, lamellarity on the size calculated via wavelength exponent spectrum analysis. We did this by simulating a set of turbidity spectra ($\lambda = 400$–600 nm) for

[4] Both error estimates were calculated for vesicles with diameter ≤120 nm studied in the wavelength range $\lambda = 400$–600 nm.

[5] It is noteworthy that keeping the mass concentration constant and increasing vesicle lamellarity reduces the number concentration of spherical shells/vesicles; turbidity increase is thus greater if the number rather than mass concentration is fixed.

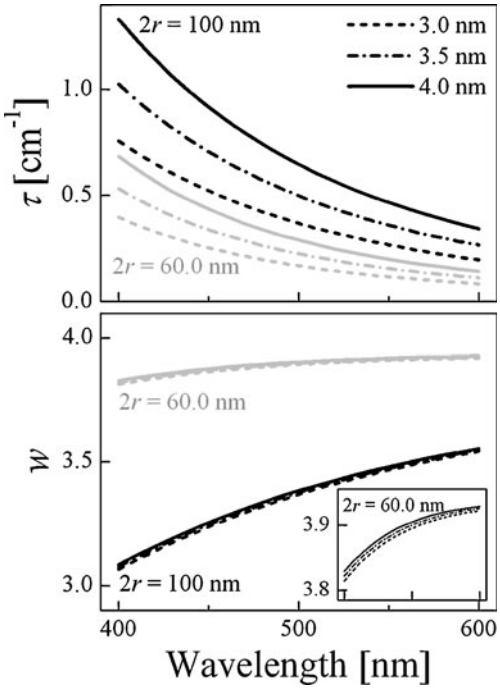

Fig. 6 Effect of spherical shell/lipid bilayer thickness ($d_b = 3$–4 nm) on turbidity (*upper panel*) and wavelength exponent (*lower panel*) of a suspension of monodisperse unilamellar lipid vesicles. The curves were calculated assuming constant lipid (dipalmitoylphosphatidylcholine) concentration of 5 mM (≈ 0.37% w/w) and shell/vesicle outer diameter $2r_v =$ 100 nm (*black curves*) or $2r_v = 60$ nm (*grey curves*). The lipid (dipalmitoylphosphatidylcholine) refractive index was calculated from Eq. D1 and the dispersion medium (water) refractive index from Eqs. C1–C2. Inset to the lower panel: blow-up of the curves pertaining to the 60 nm vesicles.

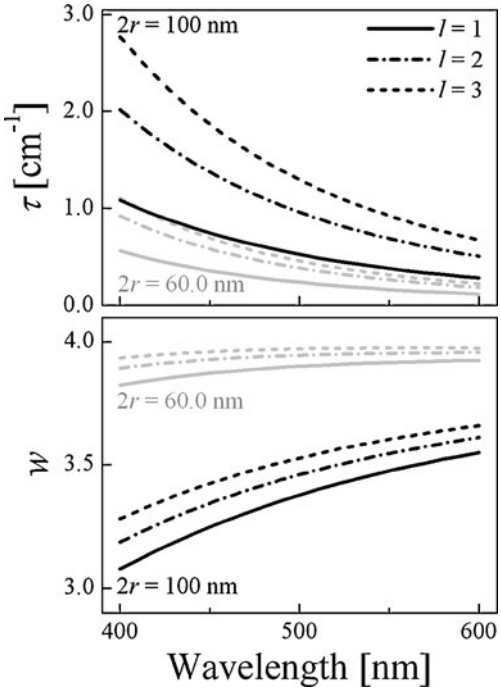

Fig. 7 Effect of lamellarity ($l = 1$, 2, or 3) on turbidity (*upper panel*) and wavelength exponent (*lower panel*) of a suspension of monodisperse lipid vesicles. The curves were calculated assuming a constant lipid (dipalmitoylphosphatidylcholine) concentration of 5 mM (≈ 0.37% w/w), bilayer thickness $d_b = 3.6$ nm, inter-bilayer/inter-shell water layer thickness $d_w =$ 3.0 nm, outer diameter $2r_v = 100$ nm (*black curves*) or $2r_v = 60$ nm (*grey curves*), lipid (dipalmitoylphosphatidylcholine) refractive index calculated from Eq. D1, and dispersion medium (water) refractive index calculated from Eqs. C1–C2.

suspensions containing unilamellar-bilamellar or unilamellar-trilamellar vesicle mixtures. We then used the simulated spectra to back-calculate the apparent vesicle diameter via wavelength exponent analysis, presuming that all vesicles are unilamellar.

Fig. 8 illustrates the resulting analytical error as a function of the weight-fraction of oligolamellar vesicles. The analytical approach underestimates the average vesicle size when oligolamellar vesicles existence is neglected. The error is small: for a suspension containing 20 weight-% bilamellar or trilamellar vesicles, the resulting mistake is below 4.0% for vesicles with a real diameter $2r_v = 60$ nm or 100 nm. One can therefore reliably derive size of lipid vesicles in suspension from wavelength exponent spectrum presuming unilamellarity even if the studied suspension actually contains a moderate fraction of oligolamellar vesicles. In turn, one can inspect oligo- or pluri-lamellarity by, first, calculating the average vesicle size from the wavelength exponent spectrum and, second, using this result to derive lamellarity from the corresponding turbidity spectrum (turbidity spectra are, in contrast to wavelength exponent spectra, very sensitive to lamellarity).

Characterization of Real Lipid Vesicle Suspensions

We investigated the practical feasibility of the analytical approach described and advocated in previous sections. Hollow spheres are more difficult to characterize with the visible light scattering than homogeneous spheres due to

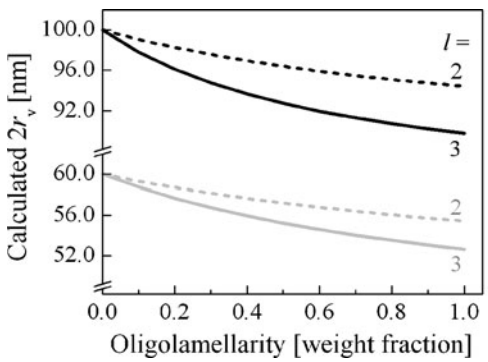

Fig. 8 Vesicle diameter calculated from wavelength exponent spectra ($\lambda = 400$–600 nm) presuming unilamellarity as a function of the weight fraction of oligolamellar vesicles. Model parameter values are the same as for Fig. 7.

their greater complexity and lower optical contrast. We therefore decided to test the proposed method with fluid-chain lipid vesicles (liposomes) rather than with homogeneous spheres. For this purpose, we prepared differently sized soybean phosphatidylcholine vesicles by extrusion, which typically yields unilamellar vesicles with a narrow size distribution (62–64). For each of the resulting suspensions, we recorded the turbidity spectrum and derived the vesicle size by analyzing the corresponding wavelength exponent spectrum. For comparison, we also characterized each suspension with dynamic light scattering.

More specifically, we first derived a wavelength exponent spectrum from each turbidity spectrum by numerically taking the derivative $-\mathrm{d}\log\tau/\mathrm{d}\log\lambda$ (Eq. 14). We then analyzed the derived wavelength exponent spectrum, $w(\lambda)$, within the framework of the Rayleigh-Gans-Debye approximation, via non-linear regression as described in the Theory section. We principally employed the hollow sphere/spherical shell model, which best describes lipid bilayer vesicles (28,29,36,45). Given that some researchers (38,65) had previously treated vesicles as homogeneous spheres with an averaged refractive index, we tested such an approach as well.

We initially presumed that the preparations were monodisperse, i.e. we did not allow for any size distribution in the first analysis. The excellent fitting results confirmed our quasi-monodispersity assumption. The results derived relying on the hollow sphere/spherical shell model agreed with the dynamic light scattering results (Table II). Conversely, treating the studied vesicles as homogeneous spheres with an averaged refractive index gave approximately 25% too large diameter (Table II), proving inadequacy of such an assumption.

Wavelength exponent spectra are little sensitive to vesicle lamellarity and bilayer thickness. They are moreover independent of vesicle concentration. Analysis of a wavelength exponent spectrum thus provides a reliable size estimate, even when only inaccurate, but reasonable, values are available for these parameters. Conversely, turbidity spectra are very responsive to all the three listed parameters. One can thus employ sizes calculated from wavelength exponent spectra to derive information about vesicle lamellarity, bilayer thickness, and/or the average area per (lipid) molecule forming bilayers/shells through turbidity spectrum analysis. Our wavelength exponent spectrum analysis assumed vesicle unilamellarity and bilayer thickness $d_b = 3.6$ nm (30). We used an average area per lipid molecule of $A_L = 0.65$ nm^2 to calculate the vesicle number concentration according to Eqs. 6 and 19. The turbidity spectra analyses based on these values gave larger diameters than the corresponding wavelength exponent spectra analyses; this suggests that at least one of the parameter values used was too low. The discrepancy was largest for the V80 suspension and smallest for the V30 suspension (possibly due to a higher fraction of oligolamellar vesicles in the former suspension).

Table II Size Characterization of the Tested Extruded Lipid Vesicles

Preparation	Geometric mean diameter, $2\bar{r}_g$ [nm][a]		
	Dynamic light scattering	Turbidity spectroscopy[b]	
		Hollow sphere	Homogeneous sphere
V80S01	106.2 ± 1.6	101.3 ± 0.0[c,e]	128.7 ± 0.1[c,e]
V80S02	111.9 ± 3.0	108.4 ± 0.4[d,f]	138.7 ± 0.6[d,f]
V50S01	86.8 ± 0.8	83.1 ± 0.3[c,e]	103.7 ± 0.4[c,e]
V50S02	89.0 ± 0.6	86.3 ± 0.4[c,g]	108.1 ± 0.5[c,g]
V50S03	92.3 ± 0.8	92.0 ± 0.4[d,h]	115.9 ± 0.6[d,h]
V30S01	72.2 ± 0.8	71.1 ± 0.1[c,j]	87.6 ± 0.2[c,j]

[a] Results are presented as mean ± SD of at least 3 replicate measurements

[b] Diameters were derived from wavelength exponent spectra, presuming vesicle monodispersity; the calculations relied on bilayer thickness $d_b = 3.6$ nm and on the refractive indices defined by Eqs. C1–C2 (for water) and D1 (for the bilayer forming phospholipid)

[c] Spectrophotometer A, the analyzed spectrum range: 400–600 nm

[d] Spectrophotometer B, the analyzed spectrum range: 400–600 nm

[e] Lipid concentration = 4 mM

[f] Lipid concentration = 3–6 mM

[g] Lipid concentration = 7–10 mM

[h] Lipid concentration = 4–10 mM

[j] Lipid concentration = 6 mM

Petrache *et al.* (40) reported for egg-yolk phosphatidylcholine $V_L = 1.2606$ nm^3 and estimated molecular area to be $A_L = 0.694$ nm^2. These values inserted into the Luzzati formula gave $d_b = 3.63$ nm, but the same authors also calculated $d_b = 4.52$ nm with a different approach. We took the quoted V_L value as a surrogate for the otherwise still unknown volume of a soybean phosphatidylcholine molecule and moreover set $3.63\,\text{nm} \leq d_b \leq 4.52$ nm. Additionally, and sensibly, assuming that V30 preparation contained merely monodisperse unilamellar vesicles, we brought results of turbidity spectrum and wavelength exponent spectrum analyses into quantitative agreement by setting $d_b = 4.1$ nm and $A_L = 0.62$ nm^2. Considering existence of oligolamellar vesicles, if real, would decrease the calculated bilayer thickness value (see Fig. 7). We thereafter ventured to assess, using the derived d_b value, vesicle lamellarity in the preparations V50 and V80. We surmised the suspensions V50 and V80 to contain unilamellar as well as bilamellar, monodisperse vesicles and repeated the analysis. This implied 11% bilamellarity in the suspension V50S01 and 24% bilamellarity in the suspension V80S01. Whilst one should take these estimates with a grain of salt, they are broadly compatible with the published information about extruded vesicles lamellarity (38,64), leaving no need for alternative explanations (e.g. by invoking vesicle non-sphericity).

To assess size distribution effects, we mixed the suspensions V80 and V50 at different ratios. We characterized the blends via wavelength exponent analyses, allowing for size distribution, and with dynamic light scattering. Table III gives the results that confirm similar sensitivity of both methods to size distribution changes. The results also support our earlier notion that analyzing wavelength exponent spectra presuming monodispersity well approximates the intensity-weighted mean diameter.

Monitoring Small Size Changes (Effect of Cholate on Size of Lipid Vesicles)

We finally checked suitability of turbidity spectroscopy for monitoring small particle, vesicle, or drug carrier size changes. To this end, we added sodium cholate to the suspensions V80 and V50 to a final surfactant concentration of 0.0−1.2 mmol/kg. We then characterized the resulting mixtures with turbidity spectroscopy, via wavelength exponent analysis, and with dynamic light scattering. The results are shown in Fig. 9 and corroborate similar sensitivity of both methods to even quite small vesicle size changes.

Experimental Recommendations and Limitations

Adjust sample concentration so that the measured optical density over the entire analyzed spectrum range lies preferably between 0.2 and 1.2. Filter all dilution media to eliminate contaminants, such as dust particles, that scatter light more than the smaller investigated particles.

To select the most appropriate wavelength range for analysis, four basic rules should be followed. First, the Rayleigh-Gans-Debye approximation criteria (see the Theory section and Appendix A) must be met at the low wavelength end. Setting the low wavelength end at $\lambda > r_v$ serves the purpose (error <10%) for typical lipid vesicles suspended in an aqueous medium. Second, the oscillating part of the inspected $w(\lambda,r)$ function must begin above the expected average particle size if the latter is to be derived from the wavelength exponent spectrum (see Appendix B). The wavelength range 400–600 nm fulfills

Table III Sensitivity of Different Analytical Methods to Changes in Vesicle Size Distribution

Sample composition	Dynamic light scattering[a]		Turbidity spectroscopy[a,b]		
V80 : V50 [w/w]	Mean diameter, $2\bar{r}_g$ [nm]	Standard deviation, σ_g^c [nm]	Mean diameter, $2\bar{r}_g$ [nm]	Standard deviation, σ_g^c [nm]	Diameter (MD)[d] [nm]
4 : 0	111.4 ± 1.3	1.4 ± 0.1 (0.11 ± 0.04)	123.2 ± 0.3	1.6 ± 0.0 (0.20 ± 0.01)	114.2 ± 0.0
3 : 1	107.0 ± 0.9	1.5 ± 0.1 (0.15 ± 0.03)	120.7 ± 1.8	1.7 ± 0.1 (0.29 ± 0.04)	110.8 ± 0.0
2 : 2	103.0 ± 1.5	1.5 ± 0.1 (0.16 ± 0.08)	109.6 ± 0.0	1.7 ± 0.0 (0.29 ± 0.00)	105.1 ± 0.0
1 : 3	97.0 ± 3.1	1.6 ± 0.4 (0.25 ± 0.24)	101.7 ± 0.1	1.8 ± 0.0 (0.36 ± 0.00)	99.3 ± 0.2
0 : 4	88.0 ± 1.1	1.4 ± 0.1 (0.12 ± 0.05)	79.6	1.4 (0.11)	84.3

[a] All calculations relied on the log normal distribution function; the given values therefore denote intensity-weighed geometric, rather than arithmetic, mean diameters and standard deviations; the results are presented as mean ± SD of replicate measurements

[b] Diameters were derived from wavelength exponent spectra; the calculations relied on the hollow sphere/spherical shell model, bilayer thickness $d_b = 3.6$ nm, and refractive indices defined by Eqs. C1–C2 (for water) and D1 (for the lipid); measurements were conducted using spectrophotometer A; Spectrum range: 400–600 nm

[c] Values between parentheses denote the conventional polydispersity index, which is defined as $\text{PI} = \delta^2 = (\ln \sigma_g)^2$

[d] Diameters calculated presuming monodispersity, i.e. not allowing for size distribution

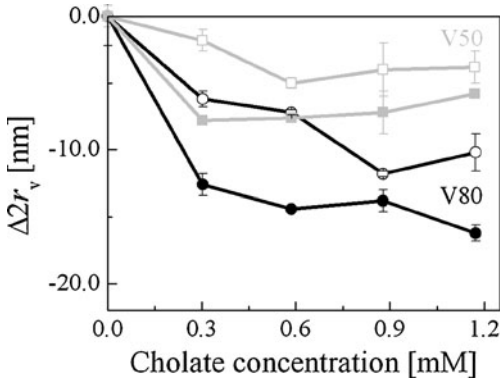

Fig. 9 Effect of sodium cholate concentration on size of extruded lipid vesicles (preparation V80 (*black circles*) and V50 (*grey squares*)), as measured with turbidity spectroscopy relying on wavelength exponent analysis (*filled symbols*) or with dynamic light scattering (*open symbols*). Analysis of wavelength exponent spectra presumed monodispersity and relied on the hollow sphere/spherical shell model, bilayer thickness d_b = 3.6 nm, and refractive indices defined by Eqs. C1–C2 (for water) and D1 (for the lipid). Results are represented as Mean ± SD.

this requirement for lipid vesicles with $2r_v \leq 150$ nm suspended in an aqueous medium. The size limit increases with the employed light wavelength. Third, the spectral region in which the tested suspension (the particles and/or the suspending medium) absorbs light significantly should be excluded from data analysis. Using $\lambda > 400$ nm is generally acceptable for vesicles comprising lipids without conjugated double-bonds. Alternatively, light absorption may be eliminated by subtraction (see (66) for the reverse procedure) to gain pure turbidity spectrum. The simplest approach to this goal is to take a difference between the spectrum measured with a turbid, absorbing suspension (e.g. prepared in water) and the corresponding spectrum of a clear, but still light absorbing, solution (e.g. prepared in water/solvent mixture). We plan to pursue such improvements in a forthcoming paper. Fourth, the signal-to-noise ratio normally governs the upper wavelength end selection; the signal-to-noise ratio is worsened as suspension turbidity decreases with increasing wavelength. Taking turbidity spectrum derivative, i.e. deriving the wavelength exponent spectrum, amplifies experimental noise. One should therefore ideally exclude the relatively "noisy" high end of a spectrum from data analysis or else smooth the spectrum before its (numerical) derivation.

Wavelength exponent spectrum analysis is typically better choice for size determination than turbidity spectrum analysis mainly because of *i*) concentration independence; *ii*) good approximation to the intensity-weighed mean diameter when presuming simplest monodispersity; *iii*) low sensitivity to shell/bilayer thickness uncertainty; *iv*) low sensitivity to number of shells/oligolamellarity. In turn, these advantages turn into disadvantages when one wishes to explore characteristics to which wavelength exponent spectrum is only moderately or not at all sensitive. Such characteristics consequently must be investigated with turbidity spectrum analysis.

CONCLUSIONS

Turbidity spectrum of submicroscopic, nanosized drug carriers in suspension contains enough information for accurate size characterization. Analysis of the wavelength exponent spectrum suffices the purpose. Other characteristics pertaining to spherical shells/vesicles, such as shell thickness and number of shells/lamellarity, can be moreover derived from turbidity spectra. In this paper, we pave the way for such applications by theoretically investigating sensitivity of turbidity spectra to various particle, vesicle and suspending medium characteristics within the framework of the RGDA. We prove the analytical approach applicability by successfully employing the proposed method to extruded lipid vesicles size and size distribution determination. The quality and kind of information derived from the measured turbidity spectra of such vesicles at least matches the outcome of the corresponding dynamic light scattering measurements. The ability of either of the two techniques to monitor small size and/or size distribution changes is also similar, but the former method offers the advantage of speed and insensitivity to suspension medium viscosity. We vindicated turbidimetric method ruggedness by recording the analyzed experimental turbidity spectra with two different spectrophotometers, which produced practically identical analytical outcome.

Our results corroborate usefulness of any good spectrophotometer for reliable nanosized drug carrier characterization. This offers a valuable new option to all researchers and scientists in pharmaceutical industry and academia—and not just to those working in specialized laboratories with dedicated equipment. Sameness of turbidity spectra may confirm directly such carrier size stability over time. Additional information about carrier size distribution or, with some restrictions, morphology (shell thickness and lamellarity for vesicles) is deducible by quantitative turbidity spectrum analysis. The unprecedented speed of the advocated method for drug carrier size characterization makes our approach suitable for assessing moderately fast kinetics. The opportunity to use a spectrophotometer equipped with a flow-through cell for continuous monitoring of drug carrier size makes the described method attractive for in-process control.

In short, the new drug carrier characterization method described in this work qualifies for routine applications in pharmaceutical research and quality control, where cost, experimental simplicity, and/or speed are of the essence.

APPENDIX A: RANGE OF VALIDITY OF THE RAYLEIGH-GANS-DEBYE APPROXIMATION

Kerker and colleagues (67) tested the range of validity of the Rayleigh-Gans-Debye approximation for homogeneous spheres by comparing the outcome of the exact Mie calculations and of the approximate calculation. The comparison included the scattering function at different angles as well as the scattering coefficient, Q_{sca}, defined as the total radiation scattered by a particle relative to the incident radiation intensity intercepted by the particle, i.e. $Q_{sca} = \tau/N_P\pi r^2$.

As we are only concerned with turbidity in this work, we present in Fig. 10 just the results for the scattering coefficient. Region I in the figure defines the range of $kr = 2\pi nr/\lambda$ and m values for which the RGDA agrees with the exact Mie theory to within 10%. In region II, the RGDA deviates from the Mie theory by no more than 100%, except in small islands where the actual deviation may be less than 10%. In region III, the error exceeds 100%.

It is noteworthy that the area just above the abscissa with $m > 1.25$ is part of region II in the originally published chart (67). The failure to obtain 10% agreement in this area is not due to limitation of the RGDA but rather due to the numerical approximation made by the authors about the refractive index, $\lim_{m\to 1} (m^2-1)/(m^2+2) = 2(m-1)/3$. The error due to this approximation is 10% at $m = 1.25$. We avoided making such an approximation in our calculations as well as in the Theory section, and consequently included the area just above the abscissa with $m > 1.25$ into region I.

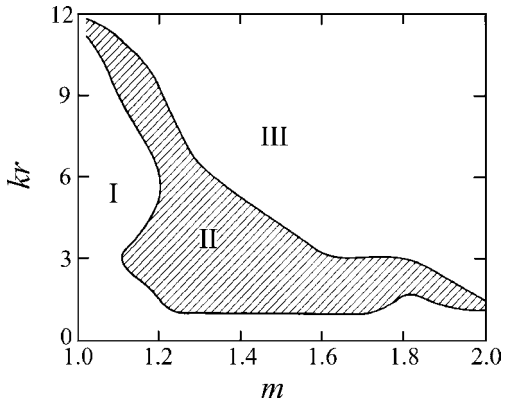

Fig. 10 The error contour chart for the scattering coefficient, Q_{sca} (modified from (45,67)). In region I, the accuracy of the Rayleigh-Gans-Debye approximation (RGDA) is better than 10%. In region II, the RGDA accuracy is between 10% and 100%, whereas in region III, the error resulting from using the RGDA exceeds 100%, except in small islands. $k = 2\pi n/\lambda$ is the propagation constant in the dispersion medium with refractive index n in which scatterers with average diameter $2r$ and refractive index n_S are dispersed. Relative refractive index is described as $m = n_S/n$.

For a suspension of homogeneous spheres with $m = 1.10$ the 10% contour line is located at $kr = 9.2$. For a suspension of homogeneous spheres in water with $m = 1.10$, the RGDA analysis of turbidity spectra is consequently correct to within 10% when $r \leq \lambda$.

APPENDIX B: RANGE OF VALIDITY OF THE ANALYTICAL APPROACH

Fig. 11 illustrates scatterer size effect on turbidity and wavelength exponent spectra over an extended range of r values. It reveals a monotonous increase of turbidity with r for homogeneous spheres and a nearly monotonous increase for vesicles. In contrast, wavelength exponent decreases with increasing scatterer size only up to certain r-limit that depends on geometry and potentially refractive index (data not shown) of the scatterer. Above such limit, wavelength exponent oscillates as a function of r, mainly owing to size-dependency of form factors. This precludes unambiguous size determination for scatterers larger than such limit based just on a non-linear regression analysis of wavelength exponent spectra. The restriction is more severe for hollow spheres, such as vesicles, than for homogeneous spheres, such as nanoparticles (Fig. 11). The r-limit generally increases with the scattered light wavelength.

Particle size derivation *via* turbidity spectrum analysis is feasible so long as the Rayleigh-Gans-Debye approximation may be applied. One can therefore employ such analysis for the particles larger than the r-limit of the otherwise more convenient wavelength exponent spectrum analysis. An even better solution is to combine turbidity and wavelength exponent spectra analyses.

APPENDIX C: THE REFRACTIVE INDEX OF WATER

The refractive index of water at 25°C under atmospheric pressure is described as a function of wavelength in the visible wavelength range with the formula

$$n_w(\lambda) = \left(\frac{2u_w(\lambda)+1}{1-u_w(\lambda)}\right)^{0.5}, \tag{C1}$$

where

$$u_w(\lambda) = b_0 + b_1\lambda^{*2} + \frac{b_2}{\lambda^{*2}} + \frac{b_3}{\lambda^{*2}-\lambda_{UV}^{*2}} + \frac{b_4}{\lambda^{*2}-\lambda_{IR}^{*2}}. \tag{C2}$$

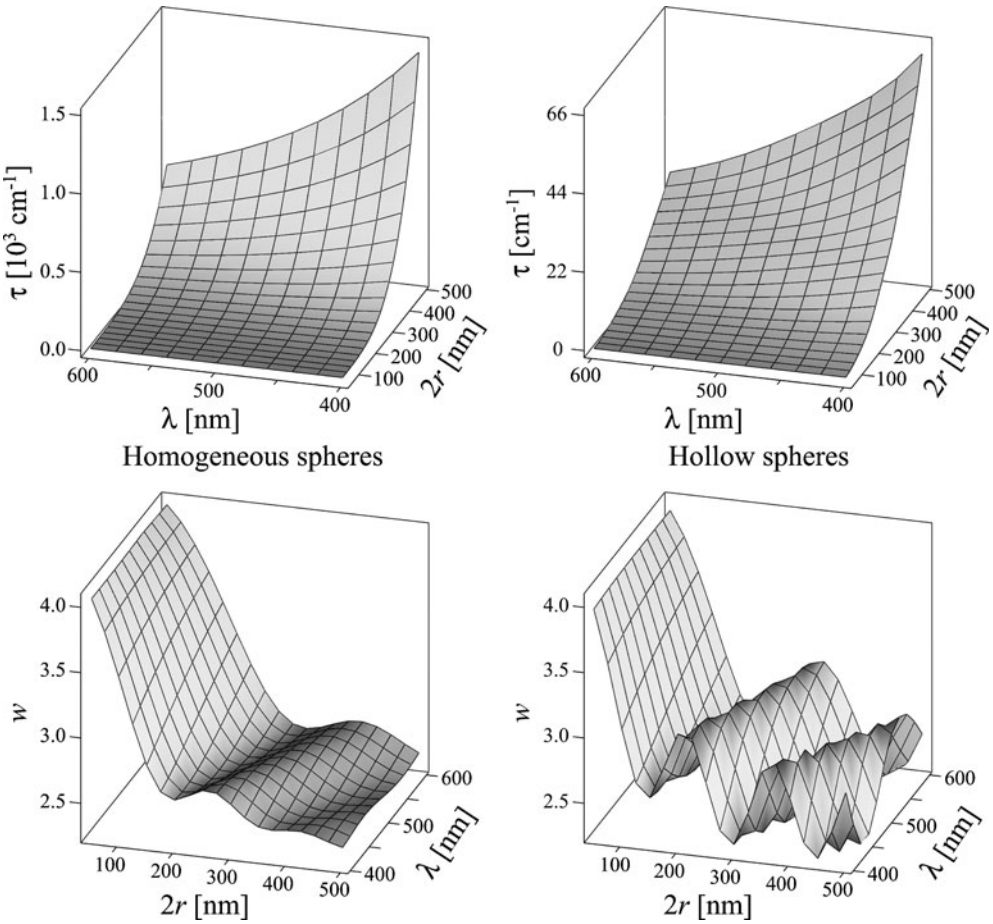

Fig. 11 Effect of the light scatterer diameter ($2r = 50.0$–500.0 nm, 25 nm intervals, monodisperse) on the scatterer suspension turbidity (*upper panels*) and wavelength exponent (*lower panels*) spectra ($\lambda = 400$–600 nm, 20 nm intervals). The curves were calculated for suspensions comprising either homogeneous spheres (*left two panels*, number concentration $N_P = 1.1 \times 10^{12}$ mL^{-1}) or hollow spheres/spherical shells/lipid vesicles (*right two panels*, number concentration $N_v = 3.5 \times 10^{13}$ mL^{-1}, shell thickness $d_{shell} = 3.6$ nm). The homogeneous spheres and the spherical shells/lipid bilayers were assumed to have the refractive index of dipalmitoylphosphatidylcholine (Eq. D1) and the dispersion medium to have the refractive index of water (Eqs. C1–C2).

$b_0 = 0.232602194$, $b_1 = +0.294685133 \times 10^{-3}$, $b_2 = +0.163176785 \times 10^{-2}$, $b_3 = +0.241520886 \times 10^{-2}$, $b_4 = +0.897025499$, $\lambda^*_{UV} = 0.2292020, \lambda^*_{IR} = 5.432937$, and $\lambda^* = \lambda/589$ nm. Eqs. C1–C2 provide absolute accuracy of $\pm 1 \times 10^{-5}$.

We derived Eqs. C1–C2 by simplifying the more general expression published by Schiebener and colleagues (68), which covers wide ranges of wavelengths, temperatures, densities, and pressures. We reached the goal by taking water density at 25°C and atmospheric pressure to be $\rho = 997.0480$ kg m^{-3} (69).

APPENDIX D: THE REFRACTIVE INDEX OF LIPID

Khlebtsov and colleagues (37) proposed the following parametric description of dipalmitoylphosphatidylcholine (DPPC) refractive index as a function of light wavelength at 20°C, based on the data measured by Chong and Colbow with visible light above 400 nm (36):

$$n_L(\lambda) = 1.4713 + 1.31\,\text{nm}\,\lambda^{-1} + 4309\,\text{nm}^2\,\lambda^{-2}. \quad \text{(D1)}$$

The result of Eq. D1 at $\lambda = 632.8$ nm, $n_L = 1.484$, compares favorably with the experimental values reported for DPPC at $T = 25$°C by Erbe and Sigl (70), $n_L = 1.478$. The result of Eq. D1 at $\lambda = 589$ nm, $n_L = 1.486$, likewise resembles acceptably the value extrapolated for DPPC to $T = 25$°C from the data published by Yi and McDonald (71), $n_L = 1.475$.

At the specified temperature, DPPC forms one particular type of the ordered-gel, L_β-phase. Eq. D1 thus does not strictly apply to any other temperature or lipid. The former restriction is especially important, as temperature not only gradually decreases n_L but moreover can trigger even more influential lipid bilayer phase transitions. Chain fluidization, for example, lowers lipid refractive index abruptly, the

reported difference for DPPC being approximately −0.008 units (71,72).

Polar lipid headgroups contribute relatively little to the refractive index difference between lipid bilayers and water. The influence of lipid chain-length and unsaturation is bigger. Both these parameters increase lipid refractive index and thus can "compete" with the temperature- and fluidization-induced n_L changes.

In all experiments reported herein we were using soybean phosphatidylcholine (SPC). This lipid has roughly two more methylene groups per chain than DPPC and contains mainly di-unsaturated chains. SPC melts below the water freezing point, and the lipid is consequently in the fluid lamellar phase, L_α, at $T=25°C$. To the best of our knowledge, results of the kind reported for DPPC by Chong and Colbow (36) are unavailable for soybean phosphatidylcholine to date. We only found some information on the refractive index of soybean oil wavelength dependency (73). Fortunately, soybean oil has arguably similar chain composition as soybean phosphatidylcholine. We therefore used the parametrization published by van Staveren and colleagues for such oil to check Eq. D1 applicability to SPC, and thus to our illustrative experimental system. Between 500 nm and 800 nm, the calculated difference between the two parametric equations amounts to -0.01203 ± 0.00084. The two underlying expressions have therefore quite similar slope $dn_L/d\lambda$ in the compared wavelength region. Van Staveren expression may not be applied below 500 nm (where it predicts $dn_L/d\lambda$ to change sign) but is essentially equivalent to Eq. D1 at longer wavelengths. We therefore applied Eq. D1 herein to cover the entire analyzed wavelength range: 400 nm$\leq\lambda\leq$ 600 nm. Shifting results of Eq. D1 downward (e.g. by subtracting the above-mentioned difference of 0.01203) from the constant in Eq. D1[6] would merely affect turbidity spectrum analysis and leave the results of wavelength exponent spectrum analysis practically unchanged. As this work has a focus on the latter option, we refrained from making such a correction herein.

Any cautious users of the analytical method advocated in this work should always check applicability of Eq. D1 to their particular experimental system. More likely than not, the expression will need to be adjusted and/or generalized. This will require knowledge of at least some reliable n_L *vs.* λ data pairs. If such information is missing, the appropriate refractive index dependency should be measured (e.g. with an Abbè refractometer). Alternatively, the n_L *vs.* λ dependency could be determined by, first, reversing the experimental sequence used in this work with the aim of generating a calibration data set for further applications. For this purpose, at least three suspensions of differently large vesicles should be prepared from the same batch of lipid and then assessed with wavelength exponent analysis and with dynamic light scattering. The results should be compared and the parameters needed for the former kind of analysis iteratively adjusted until the two size characterization methods give the same result.

[6] This means replacing in Eq. D1 the term 1.4173 with 1.4593, whilst keeping all the other parameters unchanged.

REFERENCES

1. Merisko-Liversidge E, Liversidge GG, Cooper ER. Nanosizing: a formulation approach for poorly-water-soluble compounds. Eur J Pharm Sci. 2003;18(2):113–20.
2. Chen H, Khemtong C, Yang X, Chang X, Gao J. Nanonization strategies for poorly water-soluble drugs. Drug Discov Today. 2010: In press.
3. Mäder K. Solid lipid nanoparticles as drug carriers. In: Torchilin VP, editor. Nanoparticulates as drug carriers. London: Imperial College Press; 2006. p. 187–212.
4. Mehnert W, Mäder K. Solid lipid nanoparticles: production, characterization and applications. Adv Drug Deliv Rev. 2001;47 (2–3):165–96.
5. Jones M-C, Leroux J-C. Polymeric micelles—a new generation of colloidal drug carriers. Eur J Pharm Biopharm. 1999;48(2):101–11.
6. Gutiérrez JM, González C, Maestro A, Solè I, Pey CM, Nolla J. Nano-emulsions: new applications and optimization of their preparation. Curr Opin Colloid Interface Sci. 2008;13(4):245–51.
7. Solans C, Izquierdo P, Nolla J, Azemar N, Garcia-Celma MJ. Nano-emulsions. Curr Opin Colloid Interface Sci. 2005;10(3–4):102–10.
8. Lasic DD, Barenholz Y, editors. Handbook of nonmedical applications of liposomes: from gene delivery and diagnostics to ecology. Boca Raton: CRC Press; 1996.
9. Lasic DD, Papahadjopoulos D, editors. Medical applications of liposomes. Amsterdam: Elsevier Science B.V.; 1998.
10. Peetla C, Stine A, Labhasetwar V. Biophysical interactions with model lipid membranes: applications in drug discovery and drug delivery. Mol Pharmaceutics. 2009;6(5):1264–76.
11. Fowler K, Bottomley LA, Schreier H. Surface topography of phospholipid bilayers and vesicles (liposomes) by scanning tunneling microscopy (STM). J Control Release. 1992;22(3):283–91.
12. Ruozi B, Tosi G, Leo E, Vandelli MA. Application of atomic force microscopy to characterize liposomes as drug and gene carriers. Talanta. 2007;73(1):12–22.
13. Sitterberg J, Özcetin A, Ehrhardt C, Bakowsky U. Utilising atomic force microscopy for the characterisation of nanoscale drug delivery systems. Eur J Pharm Biopharm. 2010;74(1):2–13.
14. Glatter O, Kratky O, editors. Small angle x-ray scattering. London: Academic Press; 1982.
15. Guinier A, Fournet G. Small-angle scattering of x-rays. New York: John Wiley & Sons, Inc.; 1955.
16. Svergun DI, Koch MHJ. Small-angle scattering studies of biological macromolecules in solution. Rep Prog Phys. 2003;66 (10):1735–82.
17. Augsten C, Kiselev MA, Gehrke R, Hause G, Mäder K. A detailed analysis of biodegradable nanospheres by different techniques—a combined approach to detect particle sizes and size distributions. J Pharm Biomed Anal. 2008;47(1):95–102.
18. Kiselev MA, Zemlyanaya EV, Aswal VK, Neubert RHH. What can we learn about the lipid vesicle structure from the small-angle neutron scattering experiment? Eur Biophys J. 2006;35(6):477–93.

19. Brzustowicz MR, Brunger AT. X-ray scattering from unilamellar lipid vesicles. J Appl Crystallogr. 2005;38(1):126–31.
20. Pecora R, editor. Dynamic light scattering: applications of photon correlation spectroscopy. New York: Plenum Press; 1985.
21. Hallett FR, Watton J, Krygsman P. Vesicle sizing: number distributions by dynamic light scattering. Biophys J. 1991;59 (2):357–62.
22. Ostrowsky N. Liposome size measurements by photon correlation spectroscopy. Chem Phys Lipids. 1993;64(1–3):45–56.
23. Guinier A. X-ray diffraction in crystals, imperfect crystals and amorphous bodies. San Francisco: W. H. Freeman and Company; 1963.
24. Zimm BH. The scattering of light and the radial distribution function of high polymer solutions. J Chem Phys. 1948;16 (12):1093–9.
25. Zimm BH. Apparatus and methods for measurement and interpretation of the angular variation of light scattering; preliminary results on polystyrene solutions. J Chem Phys. 1948;16(12):1099–116.
26. Jin AJ, Huster D, Gawrisch K, Nossal R. Light scattering characterization of extruded lipid vesicles. Eur Biophys J. 1999;28(3):187–99.
27. Pencer J, White GF, Hallett FR. Osmotically induced shape changes of large unilamellar vesicles measured by dynamic light scattering. Biophys J. 2001;81(5):2716–28.
28. Pencer J, Hallett FR. Effects of vesicle size and shape on static and dynamic light scattering measurements. Langmuir. 2003;19 (18):7488–97.
29. Van Zanten JH, Monbouquette HG. Characterization of vesicles by classical light scattering. J Colloid Interface Sci. 1991;146 (2):330–6.
30. Van Zanten JH, Monbouquette HG. Phosphatidylcholine vesicle diameter, molecular weight and wall thickness determined by static light scattering. J Colloid Interface Sci. 1994;165(2):512–8.
31. Korgel BA, van Zanten JH, Monbouquette HG. Vesicle size distributions measured by flow field-flow fractionation coupled with multiangle light scattering. Biophys J. 1998;74(6):3264–72.
32. Heller W. Theoretical investigations on the light scattering of spheres. XV. The wavelength exponents at small α values. J Chem Phys. 1964;40(9):2700–5.
33. Heller W, Bhatnagar HL, Nakagaki M. Theoretical investigations on the light scattering of spheres. XIII. The "wavelength exponent" of differential turbidity spectra. J Chem Phys. 1962;36(5):1163–70.
34. Heller W, Klevens HB, Oppenheimer H. The determination of particle sizes from tyndall spectra. J Chem Phys. 1946;14(9):566–7.
35. Heller W, Vassy E. Tyndall spectra, their significance and application. J Chem Phys. 1946;14(9):565–6.
36. Chong CS, Colbow K. Light scattering and turbidity measurements on lipid vesicles. Biochim Biophys Acta. 1976;436(2):260–82.
37. Khlebtsov BN, Kovler LA, Bogatyrev VA, Khlebtsov NG, Shchyogolev SY. Studies of phosphatidylcholine vesicles by spectroturbidimetric and dynamic light scattering methods. J Quant Spectrosc Radiat Transfer. 2003;79–80:825–38.
38. Matsuzaki K, Murase O, Sugishita K, Yoneyama S, Akada K, Ueha M, *et al.* Optical characterization of liposomes by right angle light scattering and turbidity measurement. Biochim Biophys Acta. 2000;1467(1):219–26.
39. Khlebtsov BN, Khanadeev VA, Khlebtsov NG. Determination of the size, concentration, and refractive index of silica nanoparticles from turbidity spectra. Langmuir. 2008;24(16):8964–70.
40. Petrache HI, Tristram-Nagle S, Nagle JF. Fluid phase structure of EPC and DMPC bilayers. Chem Phys Lipids. 1998;95(1):83–94.
41. Balgavý P, Dubnicková M, Kucerka N, Kiselev MA, Yaradaikin SP, Uhríková D. Bilayer thickness and lipid interface area in unilamellar extruded 1,2-diacylphosphatidylcholine liposomes: a small-angle neutron scattering study. Biochim Biophys Acta. 2001;1512(1):40–52.
42. Kučerka N, Gallová J, Uhríková D, Balgavý P, Bulacu M, Marrink S-J, *et al.* Areas of monounsaturated diacylphosphatidylcholines. Biophys J. 2009;97(7):1926–32.
43. Cevc G, editor. Phospholipids handbook. New York: Marcel Dekker, Inc.; 1993.
44. Mie G. Beiträge zur Optik trüber Medien, speziell kolloidaler Metallösungen. Ann Phys. 1908;25:377–445.
45. Kerker M. The scattering of light and other electromagnetic radiation. New York: Academic Press; 1969.
46. van de Hulst HC. Light scattering by small particles. New York: Dover Publications; 1981.
47. Heller W, Nakagaki M, Wallach ML. Theoretical investigations on the light scattering of colloidal spheres. V. Forward scattering. J Chem Phys. 1959;30(2):444–50.
48. Van Zanten JH. Characterization of vesicles and vesicular dispersions via scattering techniques. In: Rosoff M, editor. Vesicles. New York: Marcel Dekker, Inc.; 1996. p. 239–94.
49. Rayleigh L. On the diffraction of light by spheres of small relative index. Proc R Soc Lond A. 1914;90(617):219–25.
50. Rayleigh L. On the scattering of light by spherical shells, and by complete spheres of periodic structure, when the refractivity is small. Proc R Soc Lond A. 1918;94(660):296–300.
51. Kerker M, Kratohvil JP, Matijević E. Light scattering functions for concentric spheres. Total scattering coefficients, $m_1 = 2.1050$, $m_2 = 1.4821$. J Opt Soc Am. 1962;52(5):551–61.
52. Pecora R, Aragón SR. Theory of light scattering from hollow spheres. Chem Phys Lipids. 1974;13(1):1–10.
53. Tenchov BG, Yanev TK, Tihova MG, Koynova RD. A probability concept about size distributions of sonicated lipid vesicles. Biochim Biophys Acta. 1985;816(1):122–30.
54. Tenchov BG, Yanev TK. Weibull distribution of particle sizes obtained by uniform random fragmentation. J Colloid Interface Sci. 1986;111(1):1–7.
55. Nasner A, Kraus L. Quantitative Bestimmung von Phosphatidylcholin mit Hilfe der HPLC. Fette Seifen Anstrichm. 1981;83 (2):70–3.
56. Grit M, Crommelin DJA, Lang J. Determination of phosphatidylcholine, phosphatidylglycerol and their lyso forms from liposome dispersions by high-performance liquid chromatography using high-sensitivity refractive index detection. J Chromatogr. 1991;585(2):239–46.
57. Elsayed MMA, Cevc G. The vesicle-to-micelle transformation of phospholipid–cholate mixed aggregates: a state of the art analysis including membrane curvature effects. Biochim Biophys Acta. 2011;1808(1):140–53.
58. Provencher SW. CONTIN: a general purpose constrained regularization program for inverting noisy linear algebraic and integral equations. Comput Phys Commun. 1982;27(3):229–42.
59. Provencher SW. A constrained regularization method for inverting data represented by linear algebraic or integral equations. Comput Phys Commun. 1982;27(3):213–27.
60. Pereira G, Moreira R, Vázquez MJ, Chenlo F. Kinematic viscosity prediction for aqueous solutions with various solutes. Chem Eng J. 2001;81(1–3):35–40.
61. Wang T, Bai T-C, Wang W, Zhu J-J, Zhu C-W. Viscosity and activation parameters of viscous flow of sodium cholate aqueous solution. J Mol Liq. 2008;142(1–3):150–4.
62. Mayer LD, Hope MJ, Cullis PR. Vesicles of variable sizes produced by a rapid extrusion procedure. Biochim Biophys Acta. 1986;858(1):161–8.

63. Hope MJ, Bally MB, Webbb G, Cullis PR. Production of large unilamellar vesicles by a rapid extrusion procedure. Characterization of size distribution, trapped volume and ability to maintain a membrane potential. Biochim Biophys Acta. 1985;812(1):55–65.
64. Schmiedel H, Almásy L, Klose G. Multilamellarity, structure and hydration of extruded POPC vesicles by SANS. Eur Biophys J. 2006;35(3):181–9.
65. Yoshikawa W, Akutsu H, Kyogoku Y. Light-scattering properties of osmotically active liposomes. Biochim Biophys Acta. 1983;735 (3):397–406.
66. Castanho MARB, Santos NC, Loura MS. Separating the turbidity spectra of vesicles from the absorption spectra of membrane probes and other chromophores. Eur Biophys J. 1997;26(3):53–9.
67. Kerker M, Farone WA, Matijevic E. Applicability of Rayleigh-Gans Scattering to spherical particles. J Opt Soc Am. 1963;53 (6):758–9.
68. Schiebener P, Straub J, Sengers JMHL, Gallagher JS. Refractive index of water and steam as function of wavelength, temperature and density. J Phys Chem Ref Data. 1990;19:677–717.
69. Lide DR, editor. CRC handbook of chemistry and physics. Boca Raton: CRC Press/Taylor and Francis; 2009.
70. Erbe A, Sigel R. Tilt angle of lipid acyl chains in unilamellar vesicles determined by ellipsometric light scattering. Eur Phys J E. 2007;22:303–9.
71. Yi PN, MacDonald RC. Temperature dependence of optical properties of aqueous dispersions of phosphatidylcholine. Chem Phys Lipids. 1973;11(2):114–34.
72. Behof AF, Koza RA, Lach LE, Yi PN. Phase transitions in phosphatidylcholine dispersion observed with an interference refractometer. Biophys J. 1978;22(1):37–48.
73. van Staveren HJ, Moes CJM, van Marie J, Prahl SA, van Gemert MJC. Light scattering in Intralipid-10% in the wavelength range of 400–1100 nm. Appl Opt. 1991;30(31):4507–14.